A biological fluid fiber Sagnac sensor based on SPF-PCF-SPF structure*

GUO Junqi[1,2], WANG Changle[1,2], DI Ke[1,2], LI Zhehao[1,2], LI Renpu[1,2], and LIU Yu[1,2]****

1. *Chongqing Key Laboratory of Autonomous Navigation and Microsystem, Chongqing University of Post and Telecommunications, Chongqing 400065, China*
2. *Chongqing Engineering Research Center of Intelligent Sensing Technology and Microsystem, Chongqing University of Posts and Telecommunications, Chongqing 400065, China*

(Received 9 November 2022; Revised 22 November 2022)

A biological solution concentration sensor based on a side-polished fiber (SPF) assisted fluid system is presented. The birefringence properties of the asymmetrically filled fluid in this structure and the relationship between the concentration of the biological solution and the refractive index are theoretically analyzed. It was found that the interference peaks had red-shifted with increasing concentration. A sensing sensitivity of $1.387\ 1\times10^{4}$ nm·mL/mol at 14.68×10^{-4} mol/mL was achieved within the experimental range after different concentrations of arginine solutions were injected into the sensing system. This sensing system can also be applied to measure the concentration of other biological solutions, providing the feasibility of real-time detection of biological solutions.

Document code: A **Article ID:** 1673-1905(2023)04-0210-5
DOI https://doi.org/10.1007/s11801-023-2189-8

Biological solution sensing has received deep attention and is widely used in environmental monitoring, fermentation technology, clinical medicine and other fields[1-4]. Optic fiber sensors have the advantages of small size, high sensitivity, strong corrosion and fast response speed, which are suitable for the biological solution detection[5-7]. In recent years, many innovations have been made in fluid-filling technology that fills fluid materials into special fibers and interacts with transmitted light[8-10]. However, current fluid filling techniques require the introduction of materials into the optical fiber in advance, which cannot be replaced, updated or mixed, limiting the development in field of biological sensing[11-13]. Therefore, it is significant to design a real-time fluid control optical fiber sensor with simple structure, easy operation and high sensitivity for detecting biological characteristics, and one good solution is an optical fiber fluid sensing system.

In recent years, optical fiber-based biosensors and fluidic sensors have attracted attention from researchers. MA et al[14] designed a high-order mode (E_{21}^{y}) biological sensing structure, which is composed of a suspended racetrack micro-resonator (SRTMR) and a microfluidic channel. To analyze the mode confinement property, they calculated the confinement factors in core and cladding of the suspended waveguide and found the high-order mode could improve the sensitivity. However, the sensing sensitivity of this method is lower than that of other methods and more progress is needed. PRABHAKAR et al[15] investigated diverse single/multiple-bend waveguides, i.e. U-shaped/C-shaped/S-shaped/spiral-polymer waveguides coupled with the microchannel-network for chemical/biological-sensing functions. In the current approach, they explored the enhanced efficiency of different designs of embedded-tapered-waveguide-probe. The evanescent-field-absorbance sensitivity of embedded-tapered-waveguides was 11% superior, although both side-surfaces of the tapered-waveguide were interacting with the analyte solution. The devices required that proper waveguide-surface-modification procedure was executed. GUO et al[16] designed an optical fiber DNA sensor based on side-polish fiber, which used the photonic band gap effect to sense the concentration of the DNA solutions. The experiment used drift at the photonic bandgap boundary to detect concentration, but the use of this sensor is limited by the requirement that the injected solution's refractive index should be higher than the base in order to produce the photonic bandgap effect. In summary, the current optical fiber biosensing and fluid sensing have achieved certain research results, but the fluid channels are usually small, the fabrication of fiber sensing structures is complicated and there are many sensing constraints, limiting the technology's applications.

This work describes an optical fiber fluid sensor that measures biological solution concentrations using Sagnac interferometer. According to theory and simulations,

* This work has been supported by the National Natural Science Foundation of China (Nos.61705027, 62005033, 11704053 and 52175531), the Basic Research Project of Chongqing Science and Technology Commission (No.CSTC-2020jcyj-msxm0603), and the Science and Technology Research Program of Chongqing Municipal Education Commission (No.KJQN202000609).
** E-mails: lirp@cqupt.edu.cn; liuyu@cqupt.edu.cn

a Sagnac interferometer can observe birefringence when fluids asymmetrically filled the air holes of a photonic crystal fiber (PCF). Different concentrations of arginine solutions were used in experiments with apertures created by the side-polished fiber (SPF). Different concentrations of arginine solutions entered the air holes of the PCF through the openings provided by the SPF, and the interference peak shifts were noticed. For arginine concentrations in the range from 4.25×10^{-4} mol/mL to 24.63×10^{-4} mol/mL, a sensing accuracy of $1.387\ 1\times10^{4}$ nm·mL/mol at 14.68×10^{-4} mol/mL was attained.

Fluid sensing system employs two unique fibers (SPF and PCF). SPF is made by polishing a part of single-mode fiber. One of the primary processes for creating SPFs is mechanical grinding. The novel optical fiber known as PCF has several special features and is used in many different optical systems. The cladding's air holes can be shaped to fit the needs of the research or filled to alter the characteristics.

Fig.1 depicts the structure for fluid sensing system. The SPF supplied gap serves as a conduit for fluid to enter the PCF. The PCF used in this paper is a microstructure fiber (PCF-125-03) produced by Wuhan Changfei Optical Fiber Co., Ltd., and the cross-section is shown in Fig.2(a) and (c). The air holes in the cladding have a five-layer structure, regularly spaced array of square hexagons, each with a hole diameter of 3.5 μm and 4.9 μm between them. The polishing depth of the SPF determines the quantity of air holes that leak from the PCF. The polishing depth is 57 μm, which is just enough to leak out the five layers of air holes (blue air holes) in the PCF as shown in Fig.2(b).

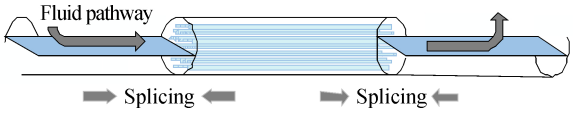

Fig.1 Schematic diagram of the fluid structure

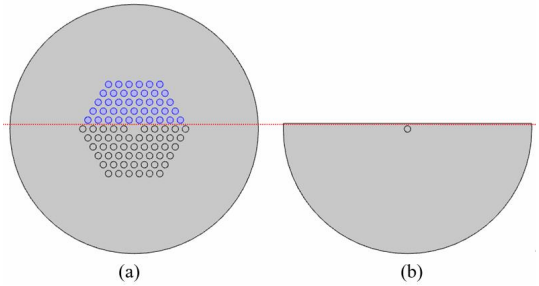

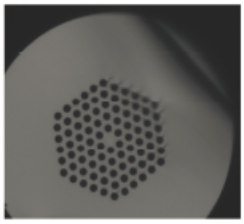

(c)

Fig.2 (a) Cross-section of PCF; (b) Diagram of SPF; (c) PCF cross-section under microscope

The problem of slow fluid filling caused by smaller channels is resolved by creating bigger fluid channels with a polishing depth of 57 μm and polishing lengths on the order of centimeters. The SPFs at each end of the PCF allow fluid to enter or exit the sensor structure, enabling the real-time dynamic measurement of biological solution concentrations.

The theoretical analysis of the relationship between the solution's concentration and refractive index is conducted. According to Lorentz electron theory, Lambert's law and Beale's law, the relationship between solution refractive index n and concentration c is as follows

$$c \approx \frac{4\pi\gamma\omega}{\alpha\lambda\left(\omega_0^2-\omega^2\right)}n-\frac{4\pi\gamma\omega}{\alpha\lambda\left(\omega_0^2-\omega^2\right)}+\frac{\pi\gamma\omega}{2\alpha\lambda\left(\omega_0^2-\omega^2\right)}\frac{n^2e^2}{\mu_0^2m^2}\frac{\left(\omega_0^2-\omega^2\right)^2-\gamma^2\omega^2}{\left(\omega_0^2-\omega^2+\gamma^2\omega^2\right)^2}, \tag{1}$$

where γ is the damping coefficient of classical radiation, ω_0 is the natural frequency of the electron, ω is the frequency of incident light, λ is the wavelength in vacuum, α is a constant independent of concentration, n is the number of atoms per unit volume, e is the charge of the electron, μ_0 is the relative dielectric constant of the medium, and m is the mass of the electron. From the above formula, the concentration and refractive indices are approximately linear when the incident light frequency is a constant.

In this paper, the arginine solutions were used for the experiments. A naturally occurring amino acid called arginine helps to strengthen the immune system and fight disease. Research has indicated that arginine can treat cardiovascular disease. It widens blood vessels, boosts blood flow, and enhances bodily circulation. In addition to improving the immune system, arginine aids in the fight against cancer cells and offers protection against viral infections. Monitoring arginine concentrations therefore is significant.

In this experiment, a total of seven sets of arginine solutions with different concentrations were prepared. Their concentrations were 4.25×10^{-4} mol/mL, 7.97×10^{-4} mol/mL, 11.05×10^{-4} mol/mL, 14.68×10^{-4} mol/mL, 17.75×10^{-4} mol/mL, 21.42×10^{-4} mol/mL and 24.63×10^{-4} mol/mL. An Abbe refractometer was used to calculate the solutions' refractive indices. At 25 °C, each concentration was measured three times, with the average value used as the result. The final graph of the arginine solution concentration and refractive index was produced, as depicted in Fig.3. The relationship between the concentration and refractive index shows a linear fit of 99.84%.

B is a crucial performance factor for estimating the birefringence. The calculation formula is the real part difference of the effective refractive index of the two polarization modes of the core as follows

$$B(\lambda)=\mathrm{Re}\left|n_{\mathrm{eff}}^{y}(\lambda)-n_{\mathrm{eff}}^{x}(\lambda)\right|, \tag{2}$$

where Re represents the real part, and $n_{\mathrm{eff}}^{x}(\lambda)$ and $n_{\mathrm{eff}}^{y}(\lambda)$ are the effective refractive indexes of the core in

the *x*-polarization and *y*-polarization, respectively.

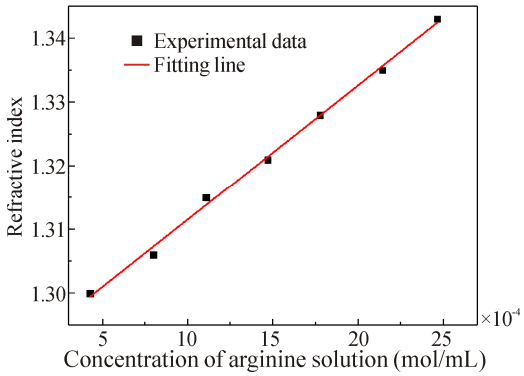

Fig.3 Relationship between arginine concentration and refractive index

The asymmetric filling of the fluid into the PCF causes the birefringence effect, and as a result, the birefringence coefficient will alter as the fluid's refractive index varies. The $n_{\mathrm{eff}}^{x}(\lambda)$ and $n_{\mathrm{eff}}^{y}(\lambda)$ in PCF filled with fluids of various refractive indices are calculated using the COMSOL Multiphysics simulation software. B is then calculated using Eq.(2). Pure silicon PCFs are used in the experiment and the birefringence is introduced by a fluid that is asymmetrically filled, thus preventing temperature interference.

The transmission interference spectrum equation is

$$\mathrm{Tr}(\lambda)=\frac{1-\cos(2\pi LB(\lambda)/\lambda)}{2}, \tag{3}$$

where L represents the length of the fluid fill, in this case which is 10 cm.

Fig.4(a) shows the Sagnac interferometer transmission spectra for the simulation of filling several fluids with varying refractive indices. The interferometric peaks are red-shifted as the refractive index increases. Fig.4(b) shows the wavelength drift curve with refractive index corresponding to the resonance peak. As the refractive index increased from 1.3 to 1.312, the wavelength is shifted by 41.6 nm with a second order fit of 99.99%. The refractive index sensing sensitivity is about 3 841.67 nm/RIU.

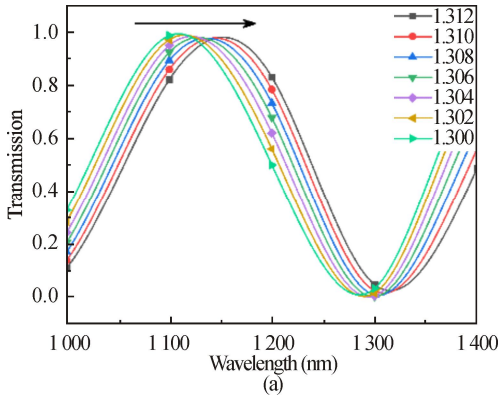

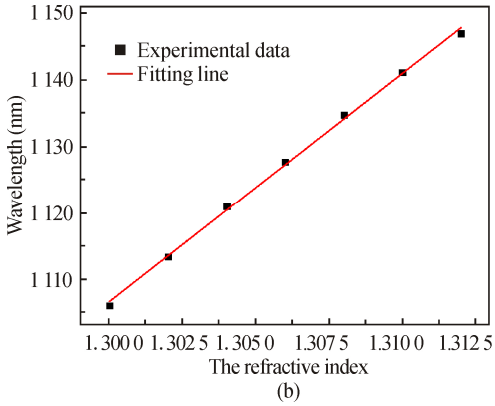

Fig.4 (a) Transmission spectra of liquid-filled fiber Sagnac interferometer with varying refractive indices; (b) RI response curve

The experimental device is shown in Fig.5, including SPF-PCF-SPF system, pressure device, tee tube, fiber coupler, polarization controller, supercontinuum light source (NKT-K90-120-00), and optical spectrum analyzer (YOKOGAWA-AQ6370D, OSA). The supercontinuum light source is connected to the 3 dB coupler and the transmitted light is divided into two beams to access both sides of SPF-PCF-SPF and polarization controller, and the output is connected to the OSA.

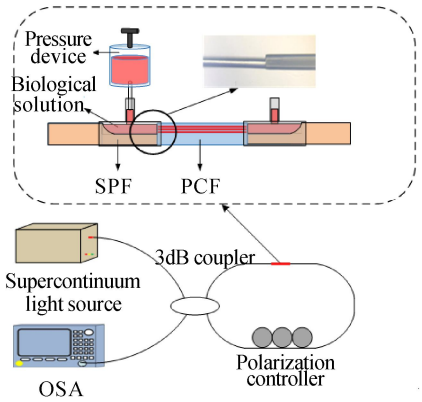

Fig.5 Schematic diagram of birefringence sensing experimental device based on Sagnac interferometer

Utilizing a pressure mechanism to force the arginine solution into the fluid channel, the sensing performance in the range of 4.25×10^{-4}—24.63×10^{-4} mol/mL is investigated. Based on the correlation between the concentration of arginine solution and the refractive index of the arginine solution, the refractive index of the arginine solution and the birefringence properties, the concentration of arginine solution can be determined from the change in wavelength of the interference peak. The interference spectrum of the filled concentration of 4.25×10^{-4} mol/mL solution is shown in Fig.6. The interference peak near 1 300 nm is selected as the observation point, and the interference peak spectra with different concentrations are shown in Fig.7. The interference peak

has red-shifted when the arginine concentration rises, which is consistent with the simulation.

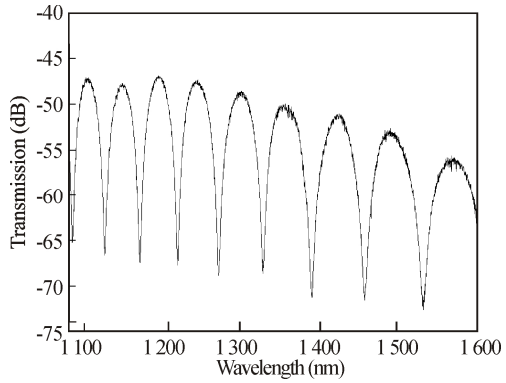

Fig.6 Transmission spectrum of the arginine solution with a concentration of 4.25×10^{-4} mol/mL

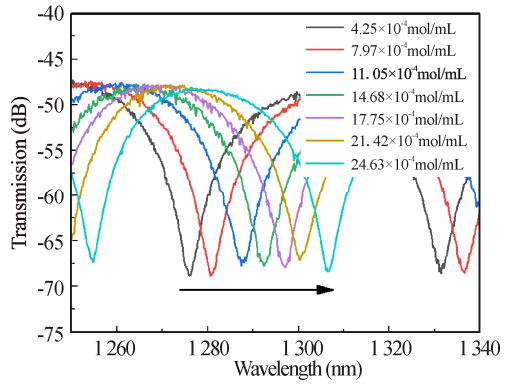

Fig.7 Concentration response characteristics of arginine solutions around 1 300 nm

The relationship between the wavelength of the interference peak and the concentration of arginine solution is displayed in Fig.8 to better analyze the sensing performance. The drift characteristics of the observation point with concentration are approximately linear. The second-order polynomial fit of 99.54% and the sensitivity of $1.387\ 1\times10^{4}$ nm·mL/mol at 14.68×10^{-4} mol/mL are achieved. The relationship between the refractive index and the concentration of arginine solution can be obtained by this relation, which provides a method to obtain the concentration of biological solution.

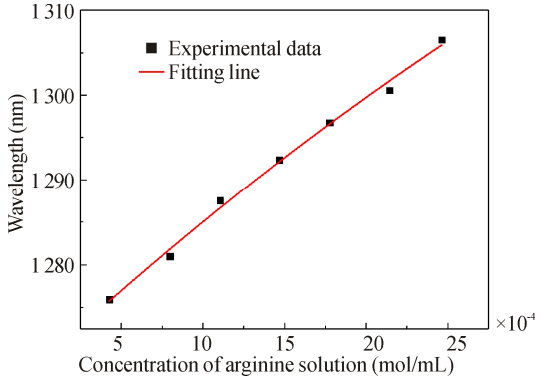

Fig.8 Arginine solution concentration response characteristics

In this paper, a novel biosensing system based on a fiber optic fluid sensing system and a Sagnac interferometer is proposed. The arginine solution is used as an example to theoretically analyze and experimentally confirm the linearity of the relationship between solution concentration and refractive index. According to the experimental findings, arginine solutions with concentrations ranging from 4.25×10^{-4} mol/mL to 24.63×10^{-4} mol/mL have a sensing sensitivity of $1.387\ 1\times10^{4}$ nm·mL/mol at 14.68×10^{-4} mol/mL. The structure is very sensitive, structurally stable, and economical. By measuring the concentration of the solution in relation to its refractive index, the technique can be used to detect the concentration of other biological solutions.

Statements and Declarations

The authors declare that there are no conflicts of interest related to this article.

References

[1] YANG F, CAO Y, LI M, et al. Refractive index and temperature optical fiber sensor based on thin core S-taper and spherical structure[J]. Optoelectronics letters, 2022, 18(6): 321-325.

[2] BOTEWAD S N, GAIKWAD D K, GIRHE N B, et al. Ultrasensitive polyaniline-nickel oxide cladding modified with urease immobilized intrinsic optical fiber urea biosensor[J]. Polymers for advanced technologies, 2022, 33(1): 189-197.

[3] LUO Y, LUO J. Experimental research on cholesterol solution concentration sensing based on tilted fiber Bragg grating[J]. Optoelectronics letters, 2021, 17(11): 661-664.

[4] LI Y, FAN H, WANG L, et al. Bend-tolerant fiber sensor based on BOTDR system[J]. Optoelectronics letters, 2022, 18(6): 343-348.

[5] MAHANI F F, MALEKI M, MOKHTARI A, et al. Design of an efficient Fabry-Perot biosensor using high-contrast slanted grating couplers on a dual-core single-mode optical fiber tip[J]. IEEE sensors journal, 2021, 21(18): 19705-19713.

[6] LI C, SONG B, WU J, et al. Dual-demodulation large-scope high-sensitivity refractive index sensor based on twin-core PCF[J]. Optoelectronics letters, 2021, 17(4): 193-198.

[7] LI X, CHEN N, ZHOU X, et al. In-situ DNA detection with an interferometric-type optical sensor based on tapered exposed core microstructured optical fiber[J]. Sensors and actuators B: chemical, 2022, 351: 130942.

[8] AYYANAR N, RAJA G T, SKIBINA Y S, et al. Hollow-core microstructured optical fiber based refractometer: numerical simulation and experimental studies[J]. IEEE transactions on nanobioscience, 2022, 21(2): 194-198.

[9] ZHANG W, BAI B B, ZHANG Y Z, et al. Sensing characteristics of near-infrared band based on new photonic

crystal fiber[J]. Chinese journal of lasers, 2021, 48(7)：0706001.

[10] YUAN T, ZHANG X, XIA Q, et al. Design and fabrication of a functional fiber for micro flow sensing[J]. Journal of lightwave technology, 2020, 39(1)：290-294.

[11] XU B, GUO Y, CHANG R, et al. Versatile interferometric sensor based on sandwiched grapefruit photonic crystal fiber[J]. IEEE sensors journal, 2021, 21(16)：17875-17881.

[12] LIN Z, ZHAO Y, LV R, et al. High-sensitivity salinity sensor based on etched C-type micro-structured fiber sensing structure[J]. Sensors and actuators A：physical, 2022, 339：113518.

[13] JIN W, ZHANG L, ZHANG X, et al. Wavelength and sensitivity tunable long period gratings fabricated in fluid-cladding microfibers[J]. Chinese physics B, 2022, 31(1)：014207.

[14] MA T, TIAN Y S, LIU S H, et al. Integrated silicon-based suspended racetrack micro-resonator for biological solution sensing with high-order mode[J]. Chinese physics B, 2021, 30(11)：114208.

[15] PRABHAKAR A, VERMA D, DHWAJ A, et al. Microchannel integrated tapered and tapered-bend waveguides, for proficient, evanescent-field absorbance based, on-chip, chemical and biological sensing operations[J]. Sensors and actuators B：chemical, 2021, 332：129455.

[16] GUO J, YANG Q, CUI W, et al. Research on a new type of biological solution fiber sensor based on hybrid-PCF[J]. IEEE sensors journal, 2021, 21(14)：16006-16014.